

Article

Dry Sliding Tribological Behavior of TC11 Titanium Alloy Subjected to the Ultrasonic Impacting and Rolling Process

Xiaohui Zhao ¹, Guilian Xue ¹ and Yu Liu ^{2,*}

¹ Key Laboratory of Automobile Materials, School of Materials Science and Engineering, Jilin University, Changchun 130025, China; zhaoxiaohui@jlu.edu.cn (X.Z.); xuegl15@mails.jlu.edu.cn (G.X.)

² School of Mechanical Science and Engineering, Jilin University, Changchun 130025, China

* Correspondence: liuyuu@jlu.edu.cn; Tel./Fax: +86-0431-8509-5316

Received: 27 October 2017; Accepted: 15 December 2017; Published: 29 December 2017

Abstract: The dry sliding friction and wear behaviors of TC11 titanium alloy subjected to the ultrasonic impacting and rolling process (UIRP) were studied in the present work. The microstructure of the deformation layer and the morphology of the worn surfaces were observed. The results clearly show that the wear performance of TC11 alloy after UIRP is better than that of TC11 alloy before UIRP under the same testing conditions. This can be attributed to the gradient nanostructure, work hardening, and low surface roughness of the treated surface layer. For the untreated samples, wear resistance first decreases and then increases with the increase of the sliding speed. Both the friction coefficient (FC) and wear rate reach a maximum value at a sliding speed of 478 r/min, and the corresponding worn surface is the most serious. While for UIRP treated samples, better friction and wear behaviors are obtained at a sliding speed of 478 r/min. This is because the deformation layer plays a protective role against wear.

Keywords: sliding friction and wear; titanium alloy; gradient nanostructure; ultrasonic impacting and rolling process

1. Introduction

Due to excellent strength and good corrosion resistance, titanium alloys are attractive candidate materials to fabricate components for aerospace, marine, and chemical applications [1–4]. However, titanium alloys as well as pure titanium are known for their notoriously poor tribological properties, which may limit their applicability particularly in areas involving friction and wear [5–7].

Surface nanocrystallization based on severe plastic deformation (SPD) has proven to be a very effective method for the improvement of wear resistance. Li et al. fabricated a nanocrystalline layer on the surface of a medium carbon steel sample and found that the nanocrystalline layer may reduce the effect of fatigue wear [8]. Matsui and Kakishima investigated the effect of shot-peening on wear resistance of steel in dry rolling/sliding wear tests. Results indicated that the pre-shot-peening treatment with ceramic balls could maintain the particulate solid lubricant well on the sample surface [9]. Wang et al. prepared a nanocrystalline layer of about 10 μm thick on the surface of a low carbon steel plate by means of surface mechanical attrition treatment. Experiment results showed that the friction coefficient (FC) decreases and the wear resistance increases with the existence of nanocrystalline layer [10]. Lu et al. produced a gradient nanograined surface layer by a newly developed surface mechanical grinding treatment. The gradient nanograined structure could act against sliding-induced surface roughening and delamination [11]. Tsuji et al. indicated that the wear resistance of Ti-6Al-4V alloy is significantly improved by the hardness increase on the surface layer under the action of plasma-carburizing and shot-peening [12].

As is known, the worst wear condition occurs under dry sliding friction. Titanium alloy presents an extremely high wear rate which increases rapidly with the increase of load at room temperature under dry sliding friction [13]. Some studies also showed that FC of TA19/WC-Co counterface is lower than that of both TC4/WC-Co and TC18/WC-Co counterfaces, indicating that the different types of titanium alloys have different tribological behaviors and wear mechanisms [14]. In fact, dry sliding friction behavior is mainly influenced by load, velocity, as well as the oxidation condition of the worn surface [15–17]. It is worth noting that surface roughness directly affects the friction behavior of the contact surfaces. Common SPD methods, like shot peening, usually increase surface roughness while strengthening the surface layer, which may negate the advantages brought by surface treatments [18,19].

The ultrasonic impacting and rolling process (UIRP) is a newly developed surface strengthening method. As a kind of surface severe plastic deformation method, apart from generating gradient nanostructure, work hardening effect, and residual compressive stress, it can also significantly reduce surface roughness [20]. Meaningful experimental results on the surface characteristics and fatigue properties of titanium alloy have been obtained [21,22], yet the effect of UIRP on the tribological properties of titanium alloy has not been studied. Therefore, this work investigated the friction and wear behaviors of TC11 titanium alloy subjected to UIRP.

2. Experiment

As-received TC11 titanium alloy (Chinese nomenclature) with chemical composition of 6.5% Al, 3.5% Mo, 1.5% Zr, 0.3% Si, 0.25% Fe, 0.08% C, 0.05% N, 0.012% H, 0.15% O (in wt %) was cut into a $100 \times 100 \times 12 \text{ mm}^3$ plate. UIRP was then applied to the plate following the procedure illustrated in a previous investigation (see Figure 1) [23]. UIRP (manufactured by Shanghai Science and Technology Development Co., Ltd. in Tianjin, China) parameters included static force of 600 N, vibration amplitude of $10 \text{ }\mu\text{m}$, feed rate of 3000 mm/min and stepping distance of 0.2 mm .

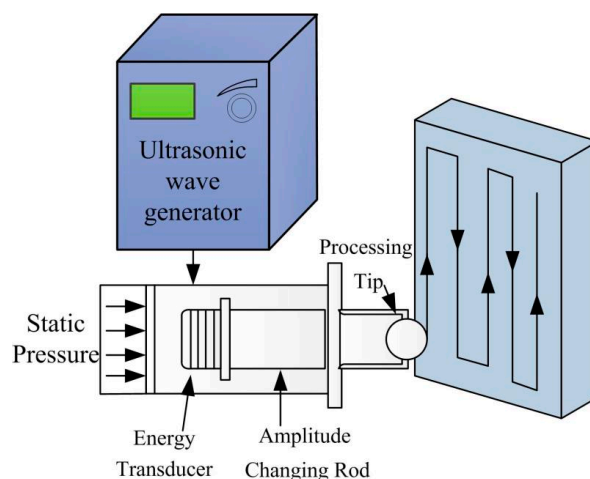


Figure 1. Schematic procedure of the ultrasonic impacting and rolling process (UIRP).

Dry sliding friction and wear experiments were performed on an MG-2000 friction and wear tester (CHENGXINSHIYANSHEBEI Limited Company, Zhangjiakou, China) with a pin-on-disk contact configuration at room temperature. Samples were cut from the UIRP plate into $\Phi 6 \times 12 \text{ mm}^3$ pins with the treated surface retained. Surface roughness (R_a) was measured to be $0.111 \text{ }\mu\text{m}$ for UIRP treated samples, while the value of the base material sample for comparison was $1.670 \text{ }\mu\text{m}$. The counter sliding part adopted in the wear tests was a GCr15 bearing steel disc with a diameter of 70 mm . The hardness of the GCr15 bearing steel disc was 500 HV , and the surface roughness was $0.890 \text{ }\mu\text{m}$.

For UIRP samples, friction and wear tests were completed undergoing 100, 200, and 300 cycles at each rotating speed. While, only a wear test of 300 cycles was carried out for original samples. Considering cyclic numbers, rotating speeds of 250 r/min, 478 r/min, and 637 r/min were used to reflect the relatively low, medium, and high sliding speeds. The radius of friction trajectory was 33 mm. The entire wear experiments were carried out with a normal load of 20 N. Samples and GCr15 disc were cleaned and dried with acetone before and after tests. Weight loss was measured on an electronic balance with accuracy of 0.01 mg, and the average value of three measurements was then taken.

Microstructure of the deformation layer was observed by JEM-2100F type of transmission electron microscopy (TEM, JEOL, Tokyo, Japan). For TEM examination, samples were sliced to a 0.3 mm thick piece strictly parallel to the treated surface, and then micro-ground to 30 μm in thickness. Subsequently, low energy ion milling was employed to complete the preparation course. The worn surface, subsurface and wear debris were examined using a VEGA3 type of scanning electron microscope (SEM, TESCAN, Brno, Czech Republic). The morphology of the cross-sections was observed with an Axio Imager A1m type of optical microscope (OM, ZEISS, Oberkochen, Germany). Hardness variation from the treated surface to the interior was determined by an MH-3 Vickers hardness tester (Shanghai Hengqi Precision Machinery Plant, Shanghai, China) with a load of 0.98 N and dwell time of 10 s. For each depth, the testing procedure was repeated five times in different positions and the average value was then adopted.

3. Results

3.1. Gradient Nanostructure Induced by UIRP

TEM bright field images of the deformation layer at different depths from the treated surface are shown in Figure 2.

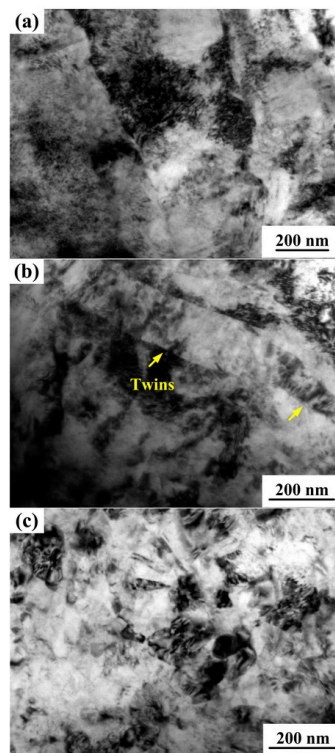


Figure 2. Transmission electron microscopy (TEM) bright field images at (a) about 120 μm below the top surface, (b) about 60 μm below the top surface, and (c) the top surface.

In Figure 2a, a large number of dislocations appear at the depth of 120 μm below the top surface, demonstrating that plastic deformation has occurred in this layer. As most dislocations gradually form dislocation tangle and dislocation cell, further plastic deformation becomes difficult as a result of the limited slip systems in the current state [23,24]. In order to coordinate deformation, twinning emerges, as shown in Figure 2b. It can be seen that at a depth of 60 μm below the top surface, the microstructure is refined, and the width of the twin bands is about 200 nm. With the continuing plastic deformation, grains are refined to nano-scale (<100 nm), as shown in Figure 2c.

3.2. Friction and Wear Properties

FCs of original samples at sliding speed of 250 r/min, 478 r/min, 637 r/min are shown in Figure 3. At the very beginning, the FCs of the original samples generally vary from 0.15 to 0.2. After that, the FC value rapidly increases to 1.1, 1.2, 1.4 corresponding to sliding speeds of 250 r/min, 478 r/min, and 637 r/min, respectively. The variation trends of FC curves at different sliding speeds are similar. For the case of 250 r/min, the first peak value of the FC curve appears with the shortest sliding distance, followed by 637 r/min and 478 r/min. The minimum stable value of the FC curve is also obtained at sliding speed of 250 r/min. At the stable stage, the FC curves for the other two cases are nearly the same. Figure 4 shows the FCs of UIRP samples at sliding speeds of 250 r/min, 478 r/min, and 637 r/min. As observed from Figure 4, the FCs of UIRP samples at different sliding speeds generally vary from 0.2 to 0.3 at the very beginning. After that, the FC curves present a relatively slow rise with slight fluctuation and become stable when the sliding distance is about 45 m. In Figure 5, a wear test of 3000 cycles was carried out for the UIRP samples under each rotating speed. It shows that the FC at sliding speed of 478 r/min is the lowest after the curves become stable.

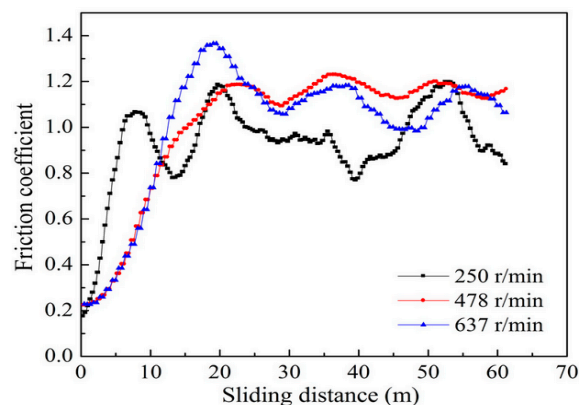


Figure 3. Friction coefficients (FCs) of original samples under different sliding speeds.

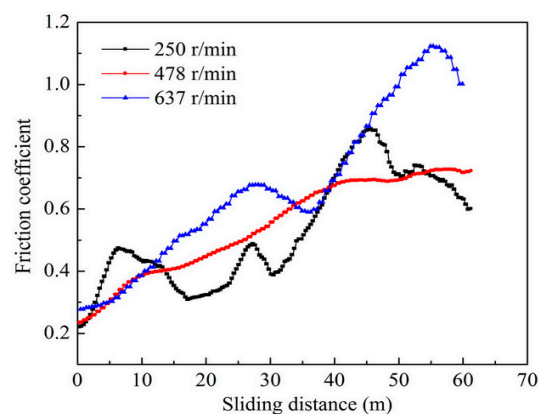


Figure 4. Friction coefficients of UIRP samples under different sliding speeds.

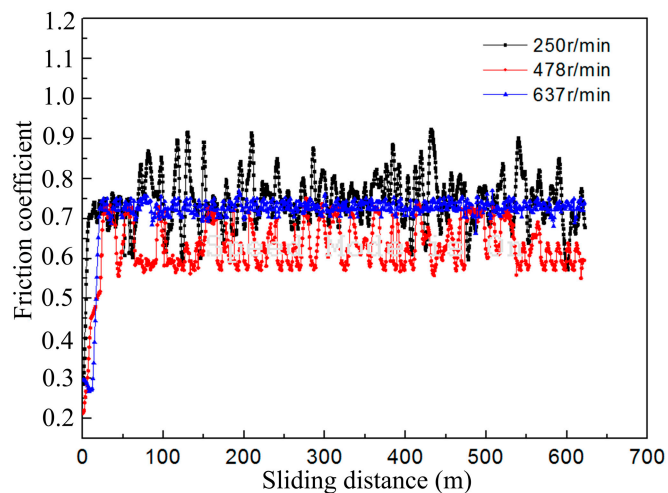


Figure 5. Friction coefficients of UIRP samples undergoing 3000 cycles at different sliding speeds.

The volume wear rates of samples before and after UIRP at different sliding speeds are shown in Figure 6. The wear distance is 62 m. It can be clearly seen from Figure 6 that the wear rate of the original samples is much higher than that of UIRP samples at any sliding speed, indicating that the wear resistance of TC11 can be improved by UIRP. The influence of sliding speed on wear rate is different for the original samples and UIRP samples. For the original samples, wear rates obtained under speeds of 478 r/min and 637 r/min are almost the same, all much larger than that under speed of 250 r/min. For UIRP samples, the wear rates increase with the continuously increasing sliding speed, and the value corresponding to 478 r/min is just slightly higher than that of 250 r/min. As the sliding speed reaches 637 r/min, the decrement of wear rate induced by UIRP declines, illustrating that the effect of UIRP on the improvement of wear resistance becomes less obvious at the higher sliding speed.

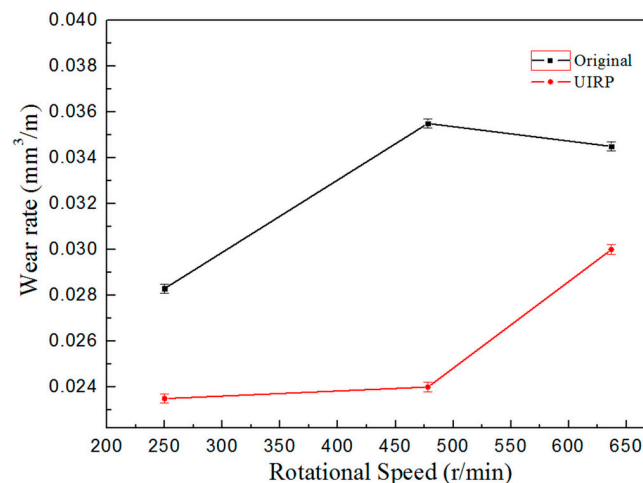


Figure 6. Comparison of wear rate between UIRP samples and original samples.

Figure 7 shows the variations of volume wear rate along with sliding distance for UIRP samples under different sliding speeds. Clearly, the wear rate reduces with the increase of the sliding distance for all cases, and within the same sliding distance, the wear rate reduces with the decrease of the sliding speed. The minimum wear rate of 0.0235 is obtained at speed of 250 r/min when the sliding distance is 62 m. While the maximum wear rate of 0.0429 is found at speed of 637 r/min when the sliding distance is 21 m. Also, the results indicate that friction surfaces deteriorate rapidly in the initial

worn period. However, this situation soon becomes better, especially for samples at high sliding speed after 200 cycles. The wear rate corresponding to 250 r/min drops more evenly.

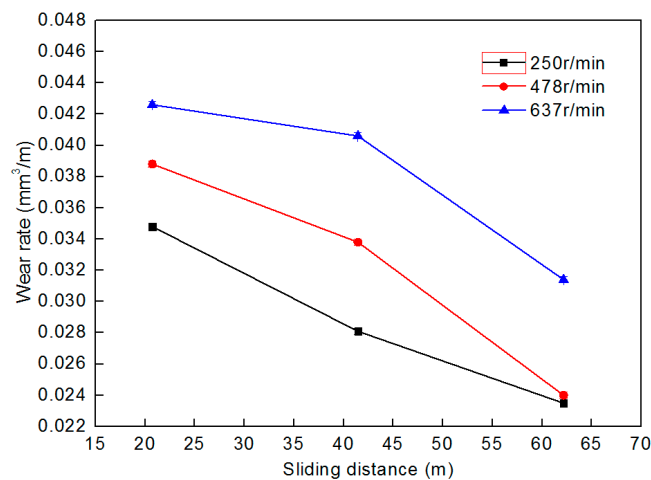


Figure 7. Wear rate of UIRP samples under different sliding speeds and sliding distances.

3.3. Morphologies of Worn Surfaces

The worn surface morphologies of UIRP and original samples at 250 r/min are shown in Figure 8. It can be seen from Figure 8a that the FC of the original sample is higher than that of the UIRP sample during the whole wear process. In the first half stage, the average of the FC for the original sample is around 1.0, while the average value for the UIRP sample is around 0.4. Even in the later stage, the former is still apparently higher than the latter. Thus, it can be inferred from the FCs that the wear of the original samples is more serious than that of the UIRP ones. Figure 8b,c show the worn surface morphologies for both kinds of samples. As observed, the UIRP surface is mainly shown as furrows and distinct adhesion traces. In contrast, the untreated surface is shown as a typical plastic deformation tear with furrows and a number of wear particles. The spalled pit in Figure 8c will soon lead to more serious lamellar tearing. Therefore, it could be concluded that the wear mechanism of the UIRP surface is adhesion wear and abrasive wear at sliding speed of 250 r/min. The wear mechanism of the untreated surface, however, is abrasive wear and delamination wear. The worn surface morphologies just correspond to the FCs of both samples, which effectively demonstrates that the tribological properties of the UIRP surfaces are better than those of untreated ones.

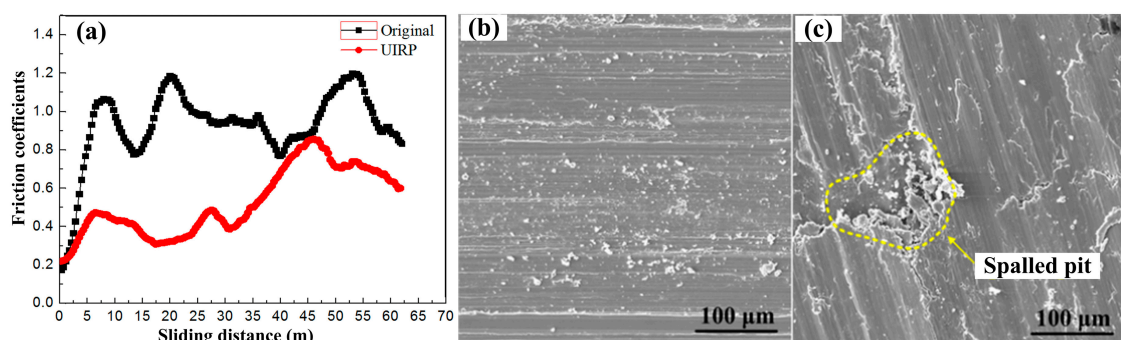


Figure 8. Friction coefficients and worn morphologies obtained at 250 r/min after 300 cycles. (a) Friction coefficients; (b) worn morphology of UIRP sample; (c) worn morphology of original sample.

The worn surface morphologies of UIRP/original samples at 478 r/min are shown in Figure 9. Though the FC curve of the UIRP sample is slightly higher than that of the original sample in the initial

short period, shown in Figure 9a, the FC of the original sample is soon up to nearly 1.2 and then enters into stable wear stage with small fluctuation. For UIRP sample, the FC gradually increases, resulting in the recession of a noticeable difference between the original sample and the UIRP one. Yet, the FC of the original sample is still larger than that of the UIRP one at later wear stage. As to worn surface morphologies, it can be seen from Figure 9b that the UIRP surface mainly presents as wear particles in dark smooth area, shallow furrows, and slight tears in local area. Thus, the wear mechanism of the UIRP surface is mainly mild oxidation wear and partial lamellar tearing. On the contrary, the main characteristic of the untreated surface (see Figure 9c) is the presence of shallow furrows and serious plastic deformation tear, which contributes to the delamination wear mechanism. Again, it is clear from the FC curves and worn morphologies that the wear resistance of the UIRP samples is better than that of the untreated ones. UIRP can certainly improve the wear performance of TC11 alloy at sliding speed of 478 r/min.

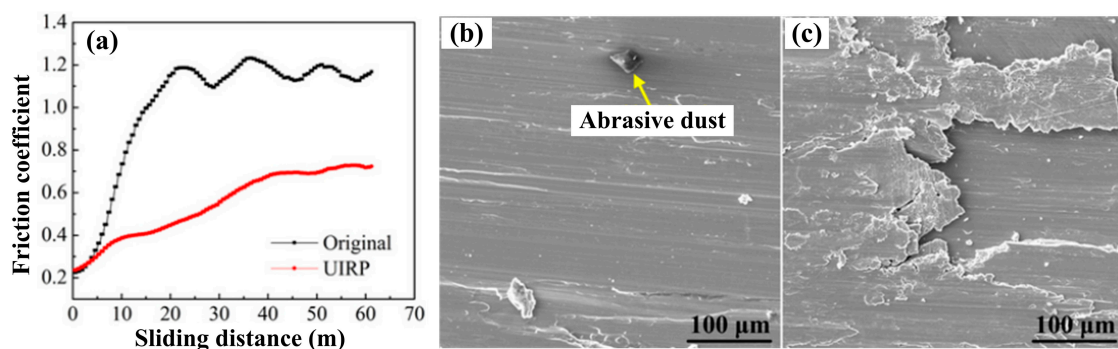


Figure 9. Friction coefficients and worn morphologies obtained at 478 r/min after 300 cycles. (a) Friction coefficients; (b) worn morphology of UIRP sample; (c) worn morphology of original sample.

Figure 10 shows the worn surface morphologies of UIRP/original samples at 637 r/min. As is shown in Figure 10a, the FC of the UIRP surface is 0.29, slightly higher than that of the untreated surface (0.21) at the beginning of the wear process. Then, the FC of the untreated surface increases rapidly to 1.4, and generally maintains at about 1.2 in the following process, while the FC of the UIRP surface increases slowly and reaches to about 1.2 until the end of the wear process.

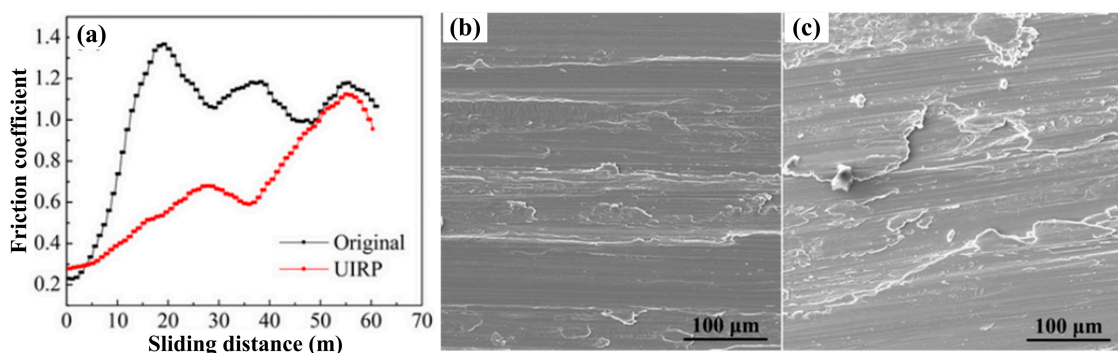


Figure 10. Friction coefficients and worn morphologies obtained at 637 r/min after 300 cycles. (a) Friction coefficients; (b) worn morphology of UIRP sample; (c) worn morphology of the original sample.

For the morphologies of the worn surfaces, wear particles, distinct furrows, and lamellar tearing in the dark smooth area can be found on the UIRP surface, while stripping wear with severe plastic deformation tear phenomenon can be found on the untreated surface. It could be concluded that UIRP can enhance the wear resistance of TC11 at sliding speed of 637 r/min. Moreover, the wear

mechanism of the UIRP samples changes from adhesion wear to oxidation wear as the sliding speed rises. The same tendency is also observed in the untreated samples, though delamination wear already occurs at 250 r/min.

Worn surface morphologies of the UIRP samples within different sliding distance at 250 r/min are shown in Figure 11. It is seen that the morphologies of the UIRP surfaces are mainly shown as furrows and adhesion traces within the scope of the investigation distance. The difference is that both furrows and adhesion traces are less at 100 cycles, while a large number of wear particles and deep furrows are observed at 200 cycles and 300 cycles. Clearly, the worn status gets worse as the friction continues and the corresponding wear mechanism of the UIRP surfaces at sliding speed of 250 r/min within different sliding distance is abrasive wear and adhesion wear.

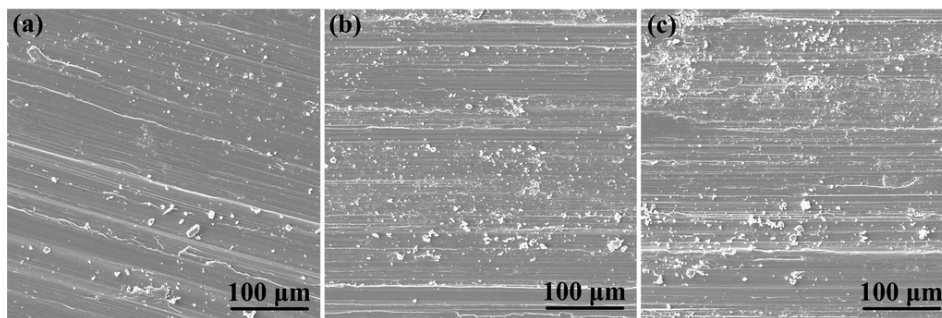


Figure 11. Worn surface morphologies of UIRP samples at 250 r/min after (a) 100 cycles, (b) 200 cycles and (c) 300 cycles.

Worn surface morphologies of UIRP samples within different sliding distance at 478 r/min are shown in Figure 12. It can be seen from Figure 12 that the morphologies of the UIRP surfaces are mainly shown as furrows with slight oxidation wear appearance in local area after 100 cycles. Wear particles in the dark smooth area and shallow furrows exist in most of the worn surfaces after 200 cycles and 300 cycles. Hence, the corresponding wear mechanism of the UIRP surfaces within different sliding distance is abrasive wear and slight oxidation wear at sliding speed of 478 r/min. Moreover, slight plastic deformation tear is also observed after 200 cycles. These tearing objects are thin and linear shaped, resulting in delamination wear.

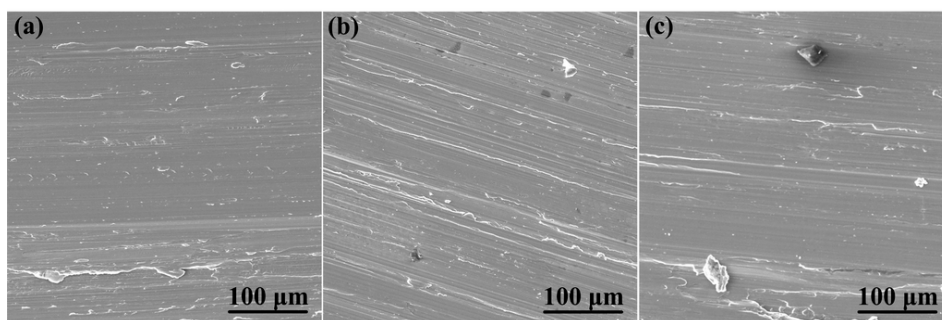


Figure 12. Worn surface morphologies of UIRP samples at 478 r/min after (a) 100 cycles, (b) 200 cycles and (c) 300 cycles.

Worn surface morphologies of UIRP samples within different sliding distance at 637 r/min are shown in Figure 13. Under sliding speed of 637 r/min, dark colored wear particles and shallow furrows exist on the worn surface of the UIRP samples after 100 cycles. Furthermore, furrows are also observed in local area. Thus, the major wear mechanism is slight oxidation wear after 100 cycles. As to 200 cycles and 300 cycles, slight plastic deformation tear is observed, as well as dark colored wear

particles, shallow furrows, and some deep furrows appearing. The corresponding wear mechanism of the UIRP samples after 200 cycles and 300 cycles is abrasive wear and slight delamination wear.

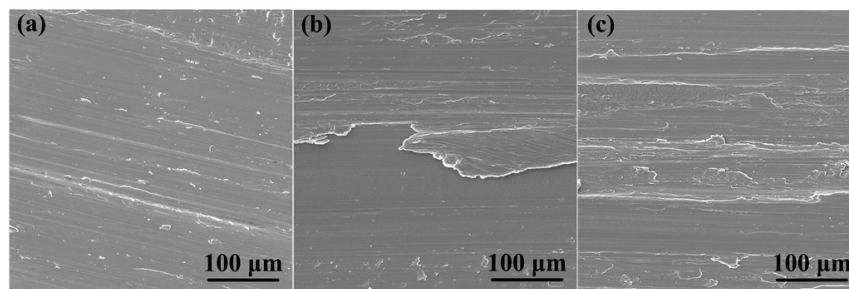


Figure 13. Worn surface morphologies of UIRP samples at 637 r/min after (a) 100 cycles, (b) 200 cycles and (c) 300 cycles.

Profile morphologies of the untreated samples are shown in Figure 14. The untreated sample surface is even without distinct plastic flow at 250 r/min, as shown in Figure 14a. The tribo-layer is more obvious and continuous at 478 r/min in Figure 14b, and the tribo-layer is further compact and continuous with plastic flow in the subsurface at 637 r/min in Figure 14c.

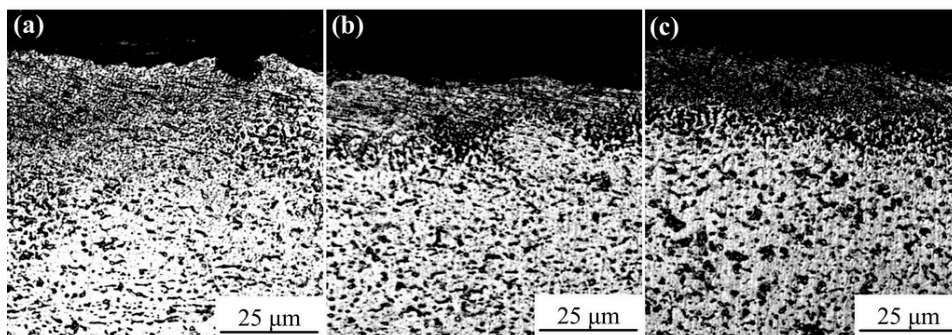


Figure 14. Profile morphologies of the untreated samples at (a) 250 r/min, (b) 478 r/min and (c) 637 r/min.

Profile morphologies of UIRP samples are shown in Figure 15. The tribo-layer on the surface of the UIRP sample at 250 r/min is not compact enough and easily peeled off, shown as Figure 15a. The tribo-layer generated at 478 r/min in Figure 15b is thicker with an obvious vortex in the worn subsurface, and it can be seen that plastic deformation also occurs on the subsurface. The tribo-layer generated at 637 r/min in Figure 15c is compact and continuous with considerable thickness.

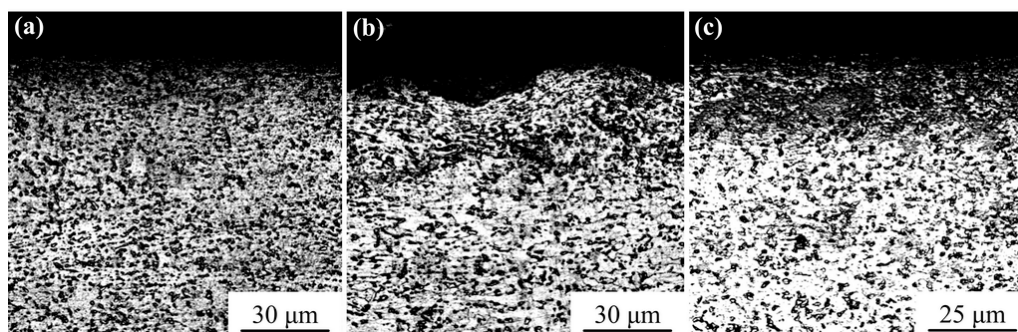


Figure 15. Profile morphologies of UIRP samples at (a) 250 r/min, (b) 478 r/min and (c) 637 r/min.

4. Discussion

The cross section microhardness of the untreated and UIRP samples after friction and wear tests is shown in Figure 16. The microhardness of the base material is about 363 HV, while the microhardness of the surface after UIRP reaches 517 HV. As is known, work hardening will occur at the sample surface due to local plastic deformation during the friction and wear process. The increased hardness will make wear resistance better in the following long period before the severely worn out stage, which is one of the important reasons why the wear rate decreases with the increase of sliding distance. Microhardness of the untreated surfaces is enhanced, and the largest increment of 32 HV occurs at sliding speed of 637 r/min. For UIRP surfaces, the largest increment is also found at 637 r/min, yet the value is about 23 HV, less than that of the untreated one. This is because the surface is already hardened during UIRP, and further work hardening caused by friction will be more difficult.

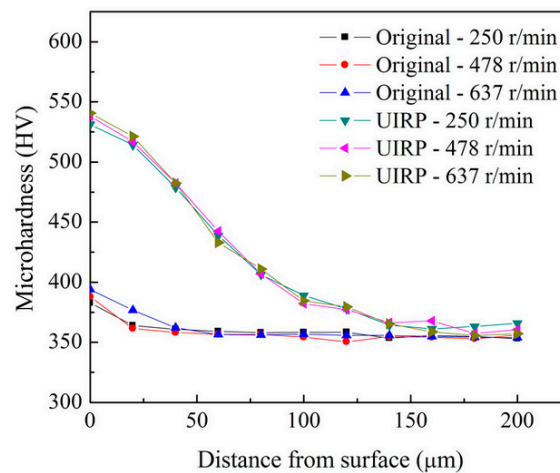


Figure 16. The cross section microhardness of UIRP and untreated samples after friction and wear tests.

Based on the above results, the influence of the sliding speed on the tribological properties of the original TC11 alloy is not monotonic. In fact, both FC and wear rate reach the maximum value at 478 r/min. Also, the wear of the surface is the most serious, and the tribo-layer of the profile morphology is not dense with obvious stripping phenomenon. The worn surface with such a serious stripping phenomenon is due to the slight oxidation film generated during friction and wear process. The unavoidable contact between the metal contact pair results in a rapid growth and an extremely high wear rate. However, Ti, Al, and other elements react with oxygen in the atmosphere and may generate Al_2O_3 , TiO_2 , and TiO , etc. at 250 r/min and 637 r/min, leading to the formation of tribo-oxide. Hence, the corresponding worn surface is better than that of 478 r/min, though stripping phenomenon is observed, especially on the worn surface at 637 r/min, whose tribo-layer is dense, continuous, and thick. It can be concluded that wear resistance of the untreated samples first decreases and then increases with the sliding speed.

On the contrary, the UIRP sample obtains relatively optimum tribological properties at 478 r/min, especially when the friction distance increases which could be seen from the comprehensive results of its FC, wear rate and worn surface morphology. Though there is not much difference between the FC value at 478 r/min and the other two cases in initial friction stage, the FC curve is indeed smoother. As to the other two cases, the worn surface at 250 r/min is slightly severer than that at 637 r/min, yet the wear rate of the former is slightly lower than that of the latter, owing to the fact that there is not enough time for wear debris to be removed from the friction system and there is reciprocating transfer from pin to disk. The debris retained in the friction system reacts with oxygen in the atmosphere to produce oxides. When the sliding speed is low, the movement of the rigid debris results in furrows on the worn surface, which cause abrasive wear. When the sliding speed is higher but the sliding

distance is lower, slight oxidation wear occurs with more gentle furrows. This can be observed from the worn surface morphologies of UIRP samples at 478 r/min and 637 r/min, yet the worn surface of the former is less than that of the latter. It is worth noting that the wear rate declines with the continuation of friction. This is because as the sliding movement between the two contact surfaces proceeds, the in-surface Ti, Al and other elements gradually react with oxygen to generate a dense oxide film containing Al_2O_3 , TiO_2 , TiO , etc., which protects the surface from being worn out.

The wear behaviors of materials before and after UIRP depend on the particular characteristics of the materials and the formation conditions of the tribo-layers. As mentioned above, the UIRP process produces gradient nanostructures, work hardening effect at the material surface, as well as reducing surface roughness. It is known that the plastic deformation capacity determines the wear resistance of materials to a great extent. TC11 alloy treated by UIRP has a very strong ability to absorb the plastic strain energy induced during the friction and wear process due to the gradient nanostructures in the surface layer. Meanwhile, the high microhardness in the surface layer also has an important role in improving wear resistance, since the tribological performance is enhanced with the increase of microhardness. Moreover, unlike most surface severe plastic deformation methods, UIRP can significantly reduce surface roughness. The low surface roughness enlarges the actual contact area between the contact pair, which weakens the adhesion effect.

5. Conclusions

The dry sliding tribological behavior of TC11 titanium alloy subjected to UIRP was studied in the present work.

The results clearly show that the wear status of TC11 alloy after UIRP is better than that before UIRP under the same testing conditions. This can be attributed to the gradient crystalline structure, the work hardening state in the surface layer, and the low surface roughness. For untreated samples, the wear resistance first decreases and then increase with the sliding speed. Both the FC and wear rate reach a maximum value at 478 r/min, and the corresponding worn surface is the most serious. While for UIRP samples, the trend is basically opposite, better results are obtained at 478 r/min.

UIRP has the potential of being a very effective method to improve friction wear performance.

Acknowledgments: The authors acknowledge the financial support by the Youth Scientific Research Fund of Jilin Province through Grant No. 20150520023JH and the National Science Foundation through Grant No. 51405182.

Author Contributions: In this work, Xiaohui Zhao and Yu Liu conceived and designed the experiments; Guilian Xue performed the experiments; Yu Liu and Guilian Xue analyzed the data; Xiaohui Zhao wrote the paper.

Conflicts of Interest: The authors declare no conflicts of interest.

References

1. Li, L.X.; Lou, Y.; Yang, L.B.; Peng, D.S.; Rao, K.P. Flow stress behavior and deformation characteristics of Ti-3Al-5V-5Mo compressed at elevated temperatures. *Mater. Des.* **2002**, *23*, 451–457. [[CrossRef](#)]
2. Wang, Q.; Zhang, P.Z.; Wei, D.B.; Wang, R.N.; Chen, X.H.; Wang, H.Y. Microstructure and sliding wear behavior of pure titanium surface modified by double-glow plasma surface alloying with Nb. *Mater. Des.* **2013**, *49*, 1042–1047. [[CrossRef](#)]
3. Du, Z.X.; Xiao, S.L.; Shen, Y.P.; Liu, J.S.; Liu, J.; Xu, L.J.; Kong, F.T.; Chen, Y.Y. Effect of hot rolling and heat treatment on microstructure and tensile properties of high strength beta titanium alloy sheets. *Mater. Sci. Eng. A* **2015**, *631*, 67–74. [[CrossRef](#)]
4. Gurrappa, I. Characterization of titanium alloy Ti-6Al-4V for chemical, marine and industrial applications. *Mater. Charact.* **2003**, *51*, 131–139. [[CrossRef](#)]
5. Alam, M.O.; Haseeb, A.S.M.A. The relationships between tribological behaviour and heat-transfer capability of Ti6Al4V alloys. *Tribol. Int.* **2002**, *35*, 357–362. [[CrossRef](#)]
6. Molineri, A.; Straffelini, G.; Tesi, B.; Baccai, T. Dry sliding wear mechanisms of the Ti6Al4V alloy. *Wear* **1997**, *208*, 105–112. [[CrossRef](#)]
7. Budinski, K.G. Tribological properties of titanium alloys. *Wear* **1991**, *151*, 203–217. [[CrossRef](#)]

8. Li, G.B.; Chen, J.; Guan, D.L. Study on mechanical properties of nano-Fe₃O₄ reinforced nitrile butadiene rubber. *Tribol. Int.* **2010**, *43*, 2216–2221. [[CrossRef](#)]
9. Matsui, M.; Kakishima, H. Improvement of tribological performance of steel by solid lubricant shot-peening in dry rolling/sliding contact wear tests. *Wear* **2006**, *260*, 669–673. [[CrossRef](#)]
10. Wang, Z.B.; Tao, N.R.; Li, S.; Wang, W.; Liu, G.; Lu, J.; Lu, K. Effect of surface nanocrystallization on friction and wear properties in low carbon steel. *Mater. Sci. Eng. A* **2003**, *352*, 144–149. [[CrossRef](#)]
11. Chen, X.; Han, Z.; Li, X.Y.; Lu, K. Lowering coefficient of friction in Cu alloys with stable gradient nanostructures. *Sci. Adv.* **2016**, *2*, e1601942. [[CrossRef](#)] [[PubMed](#)]
12. Tsuji, N.; Tanaka, S.; Takasugi, T. Effects of combined plasma-carburizing and shot-peening on fatigue and wear properties of Ti-6Al-4V alloy. *Surf. Coat. Technol.* **2009**, *203*, 1400–1405. [[CrossRef](#)]
13. Chen, K.; Zhang, Q.; Li, X.; Wang, S. Dry Sliding Wear Behavior of TC11 Alloy/GCr15 Steel Tribo-pair. *Rare Met. Mater. Eng.* **2015**, *44*, 1531–1535.
14. Niu, Q.L.; Zheng, X.H.; Ming, W.W.; Chen, M. Friction and wear performance of titanium alloys against tungsten carbide under dry sliding and water lubrication. *Tribol. Trans.* **2013**, *56*, 101–108. [[CrossRef](#)]
15. Martinez, J.M.V.; Pedemonte, F.J.B.; Galvin, M.B.; Gomez, J.S.; Barcena, M.M. Sliding wear behavior of UNS R56400 titanium alloy samples thermally oxidized by laser. *Materials* **2017**, *10*, 830. [[CrossRef](#)] [[PubMed](#)]
16. Li, X.X.; Zhou, Y.; Ji, X.L.; Li, Y.X.; Wang, S.Q. Effects of sliding velocity on tribo-oxides and wear behavior of Ti-6Al-4V alloy. *Tribol. Int.* **2015**, *91*, 228–234. [[CrossRef](#)]
17. Okonkwo, P.C.; Kelly, G.; Rolfe, B.F.; Pereira, M.P. The effect of sliding speed on the wear of steel-tool steel pairs. *Tribol. Int.* **2016**, *97*, 218–227. [[CrossRef](#)]
18. Dai, K.; Shaw, L. Comparison between shot peening and surface nanocrystallization and hardening processes. *Mater. Sci. Eng. A* **2007**, *463*, 46–53. [[CrossRef](#)]
19. Bagherifard, S.; Fernandez-Pariente, I.; Ghelichi, R.; Guagliano, M. Fatigue behavior of notched steel specimens with nanocrystallized surface obtained by severe shot peening. *Mater. Des.* **2013**, *45*, 497–503. [[CrossRef](#)]
20. Wang, T.; Wang, D.P.; Liu, G.; Gong, B.M.; Song, N.X. Investigations on the nanocrystallization of 40Cr using ultrasonic surface rolling processing. *Appl. Surf. Sci.* **2008**, *255*, 1824–1829.
21. Zhao, X.H.; Xue, G.L.; Liu, Y. Gradient crystalline structure induced by ultrasonic impacting and rolling and its effect on fatigue behavior of TC11 titanium alloy. *Results Phys.* **2017**, *7*, 1845–1851. [[CrossRef](#)]
22. Liu, Y.; Xue, G.L.; Zhao, X.H. Strain-induced gradient crystalline evolution mechanism of Ti-6.5Al-3.5Mo-1.5Zr-0.3Si during ultrasonic impacting and rolling process. *Micro Nano Lett.* **2017**, *12*, 304–307. [[CrossRef](#)]
23. Li, Y.; Sun, K.G.; Liu, P.; Liu, Y.; Chui, P.F. Surface nanocrystallization induced by fast multiple rotation rolling on Ti-6Al-4V and its effect on microstructure and properties. *Vacuum* **2014**, *101*, 102–106. [[CrossRef](#)]
24. Luo, X.T.; Wei, Y.K.; Wang, Y.; Li, C.J. Microstructure and mechanical property of Ti and Ti6Al4V prepared by an in-situ shot peening assisted cold spraying. *Mater. Des.* **2015**, *85*, 527–533. [[CrossRef](#)]

